

# How screened exchange improves on violations of the Pauli principle in the random phase approximation of jellium

P. Ziesche

*Max-Planck-Institut für Physik komplexer Systeme*

*Nöthnitzer Str. 38, D-01187 Dresden, Germany*

F. Hummel

*Institute for Theoretical Physics, TU Wien*

*Wiedner Hauptstraße 8-10, 1040 Vienna, Austria*

(Dated: August 29, 2017)

Within many-body perturbation theory (MBPT) of the spin-unpolarized homogeneous electron gas (HEG) the second order exchange term is explicitly renormalized using the random phase approximation (RPA). Regarding total energies this has been studied under the name second order screened exchange (SOSEX). We study the pair correlation function (PCF) for parallel spins to investigate to what extend the exchange terms correct for violations of the Pauli principle introduced by the RPA. The PCF evaluated in the thermodynamic limit by means of a Monte-Carlo integration of the imaginary frequency propagators of the free electron gas.

## I. INTRODUCTION

The uniform or homogeneous electron gas (HEG) is a prototypical model for a neutral metallic system assuming homogeneous positive background charge rather than atomic ions. Despite this simplification the HEG cannot be solved by finite order perturbation theory due to the far reaching character of the Coulomb interaction, which leads to divergences in all orders. However, one can arrive at a finite and meaningful result by summing over all orders of the perturbation before summing over all states occurring in the perturbation terms — a process called renormalization. Macke [1] was the first who performed that renormalization and calculated, what was later termed random phase approximation (RPA). For the HEG this recipe has been successfully applied to the total energy  $e$ , the momentum distribution  $n(k)$ , and to the structure factor  $S(q)$ . From a Fourier transform of  $S(q)$  one can obtain the pair correlation function (PCF)  $g(r)$ , which exhibits a major deficiency of the RPA rendering  $g_p(r)$  negative for small  $r$ . Due to the Pauli exclusion principle the PCF of parallel electrons is expected to be zero at the electron coalescence point  $r = 0$ . In the RPA this is, however, not the case.

As pointed out by Goldstone [15] this does not come as a surprise. Diagrams do not respect the Pauli exclusion principle individually. Violations in one type of diagram are only corrected by other diagrams of the same order but of different topology where the offending states are exchanged. In finite order perturbation theory, such as Møller–Plesset theory, all diagrams of each order can be included in order to respect the Pauli principle, however, the renormalization process of the RPA disregards exchange type diagrams entirely.

The lowest order exchange diagram beyond Hartree–Fock is of second order as shown in Fig. 2(a). It is finite and does not require renormalization as found by Onsager *et al.* [7] who calculated it even analytically (!). Screening one of the two bare Coulomb interactions yields a class of diagrams termed second order screened exchange (SOSEX) and depicted in Fig. 2(b). Total energies of the HEG in the SOSEX correction to the RPA have been studied already by Freeman [14] finding them fortuitously close to quantum Monte-Carlo (MC) total energies. Its contribution to the structure factor from the diagram in Fig. 2(c) and to what extend it improves on the violations of the Pauli principle have not been studied for the HEG so far and are subject of the present paper.

All the characteristic quantities of the HEG, such as the correlation energy  $e_{\text{corr}}$ , depend

on  $r_s$ , which is the radius of a sphere, containing on average just one electron. Particle number fluctuations beyond that are observable in the pair correlation functions  $g_{a,p}$  as functions of  $r$  and (parametrically) of  $r_s$  for electron pairs with antiparallel (a) and parallel (p) spins [2]. For a recent parametrization of  $e_{\text{corr}}(r_s)$  see [28] and in [17] results of MC calculations are analytically analyzed. The limiting case  $r_s = 0$  corresponds to the ideal Fermi gas. The above mentioned failure of MBPT makes the function  $e_{\text{corr}}(r_s)$  singular at  $r_s = 0$  with  $r_s^2 \ln r_s$ . A similar peculiar behavior is exhibited by  $n(k)$  for  $k \rightarrow 1$  and by  $S(q)$  for  $q \rightarrow 2$  from the Fermi surface.

Whereas the Coulomb hole  $g_a$ , with  $g_a(0) = 1 - \mathcal{O}(r_s)$ , arises only through the Coulomb repulsion, the larger Fermi hole  $g_p = \mathcal{O}(r^2)$  comes from the combined action of the (dominant) Pauli principle and the (correcting) Coulomb repulsion. Equivalent information is provided by the static structure factors (SFs)  $S_{a,p}(q)$ , which are obtained by the Fourier transforms of  $g_{a,p}(r)$  [3]. An analysis in terms of Feynman diagrams (see Appendix) shows, that  $S_a = S_d$  (d means "direct", to distinguish it from x="exchange"), whereas  $S_p$  splits according to  $S_p = S_p^{\text{HF}} + S_p^{\text{cum}}$  into a Hartree–Fock (HF) like part  $S_p^{\text{HF}}$  reducible to the correlated  $n(k)$  and a cumulant non-reducible remainder  $S_p^{\text{cum}}$  [3], which again splits according to  $S_p^{\text{cum}} = S_d - S_x$  into the direct part  $S_d$  and the corresponding exchange part  $S_x$ . Thus for  $S = S_a + S_p$  it is  $S = S_p^{\text{HF}} + 2S_d - S_x$ . These splittings have been derived in [4, 5] from the 2-body reduced density matrix and its linked-diagram representations. The same splitting follows automatically from the linked-diagrams of  $e_{\text{corr}}$  and the generalized Hellmann–Feynman theorem, see Eqs. (4) and (5). Note that the approximations for "HF" and "cum" have to base on the same footing.

At the level of the RPA the  $e_{\text{corr}}$  of the HEG has been studied [1, 6], [7]. It was extended to the static quantities  $n(k)$  [8, 9],  $S(q)$  [10–13], the 2-body reduced density matrix [4, 5], and also to the dynamic quantities  $G(\mathbf{k}, \omega), S(k, \omega)$  with plasmon frequency and plasmon damping [29, 30]. This paper continues [4, 5] and explains the partitioning of  $S_p$  which includes the Pauli principle and shows that RPA neglects important contributions to the spin-parallel part of the structure factor as well as to second order of  $n(k)$ , stemming from exchange effects.

### Remark on the notation

The momenta  $k = |\mathbf{k}|$  and  $q = |\mathbf{q}|$  are measured in units of  $k_F = 1/(\alpha r_s)$ , energies in  $k_F^2$ ,  $t(\mathbf{k}) = \mathbf{k}^2/2$ ,  $v(\mathbf{q}) = q_c^2/q^2$ ,  $q_c^2 = 4\alpha r_s/\pi$ ,  $\alpha = (4/9\pi)^{1/3}$ ,  $\omega_{\text{pl}}^2 = q_c^2/3$ ,  $a = (1 - \ln 2)/\pi^2 = 0.0311$  is referred to as Macke number, and  $x = (\alpha r_s)^2 \ln r_s$ . There are several functions of  $q$ , often the argument is not given explicitly for convenience, *e.g.*  $S$  means  $S(q)$ , respectively  $S(q, r_s)$ . What is in [4] named  $(1/2)F(q)$ , is here and in [5] denoted by  $F(q)$ .

## II. PAIR CORRELATION FUNCTIONS AND STRUCTURE FACTORS

We resolve the pair correlation function  $g(r)$  and the structure factor  $S(q)$  into spin-antiparallel and a spin-parallel part according to  $g = g_a + g_p$  and  $S = S_a + S_p$ , respectively. The SFs  $S_{a,p}$  are normalized according to

$$\int_0^\infty d(q^3) (-1)S_a(q) = [1 - g_a(0)], \quad \int_0^\infty d(q^3) [1 - S_p(q)] = 1, \quad (1)$$

and they contribute to the total interaction energy  $v = v_a + v_p$  with

$$v_a = \frac{3\omega_{\text{pl}}^2}{4} \int_0^\infty dq S_a(q), \quad v_p = -\frac{3\omega_{\text{pl}}^2}{4} \int_0^\infty dq [1 - S_p(q)] \quad \curvearrowright \quad v = -\frac{3\omega_{\text{pl}}^2}{4} \int_0^\infty dq [1 - S(q)] \quad (2)$$

as functions of  $r_s$ . The energy in lowest order is  $v_1 = -(3\omega_{\text{pl}}/4)$ . From the SFs  $S_{a,p}$  follow the pair correlation functions (PCFs)

$$g_a(r) = 1 + \int_0^\infty d(q^3) \frac{\sin qr}{qr} S_a(q), \quad g_p(r) = 1 - \int_0^\infty d(q^3) \frac{\sin qr}{qr} [1 - S_p(q)] \quad (3)$$

with  $g_p(0) = g'_p(0) = 0$  for the Pauli principle, which makes the exact parallel-spin PCF to start with  $g_p(r) = (1/2)g''_p(0)r^2 + \dots$ . The conservation of particles implies  $S_{a,p}(0) = 0$ . This makes also

$$\alpha^3 \int_0^\infty d(r^3) [1 - g_p(r)] = 1, \quad \int_0^\infty d(r^3) [1 - g_a(r)] = 0,$$

known as the perfect screening SR (or charge neutrality condition). Important correlation parameters are  $g_a(0)$  and  $g''_p(0)$ . As already Goldstone mentioned, it may be violated with  $g_p(0) \neq 0$ , if not all exchange processes are included. The small- $q$  limit  $S(q \rightarrow 0) = q^2/(2\omega_{\text{pl}}) + \dots$  is the plasmon SR, see refs. in [17].

The energy  $e$  is a sum of topologically distinct vacuum diagrams, each of them built up from the 1-body propagator  $G_0(\mathbf{k}, \omega)$ , which contains  $t(\mathbf{k}) = \mathbf{k}^2/2$ , and from the static (frequency independent) Coulomb repulsion  $v(\mathbf{q}) = q_c^2/\mathbf{q}^2$ . The particle-hole (p-h) lines form closed loops, linked by interaction lines. Each interaction line comes from a p-h-line and runs into another or the same p-h-line (forming thus vertices). Each closed loop appears twice according to the two spin orientations. Each vacuum diagram consists of closed loops linked by interaction lines defining thus a functional of  $t(\mathbf{k})$  and  $v(\mathbf{q})$ . Then  $n(k)$  and  $S(q)$  follow from the generalized Hellmann–Feynman theorem:

$$n(k) = \frac{\delta e}{\delta t(\mathbf{k})}, \quad t = \int_0^\infty d(k^3) n(k) \frac{k^2}{2}, \quad \int_0^\infty d(k^3) n(k) = 1, \quad (4)$$

$$S(q) = 1 + 16\pi \frac{\delta e}{\delta v(\mathbf{q})}, \quad v = -\frac{3\omega_{\text{pl}}^2}{4} \int_0^\infty dq [1 - S(q)], \quad \int_0^\infty d(q^3) [1 - S(q)] = 2[1 - g(0)]. \quad (5)$$

In Eq. (5) the differential operator cuts out successively interaction lines according to the product rule. In Eq. (4) p-h-lines are successively cut.

It is easy to show by means of Eq. (5) that the vacuum diagrams of  $e$  are transformed quite automatically to the 2-point diagrams of  $S_{d,x}$  and  $F$  as

$$S_a = S_d, \quad S_p = [1 - F] + [S_d - S_x] = S_p^{\text{HF}} + S_p^{\text{cum}}, \quad (6)$$

where the 'direct' diagrams  $S_d$  are linking **two** closed loops. The exchange diagrams  $S_x$  are as in Fig. 2(b), where the cutting procedure happens only at **one** and the same closed loop. Apart the term of Fig. 2(c) there are 2-point  $S_p$ -diagrams, which have no links between its left and right half. Such  $S_p$ -diagrams can be summed up according to  $G_0 \rightarrow G$ , indicated in Fig. 3, to give the HF-function  $F$ , where  $n(k)$  is the correlated momentum distribution [4, 5, 8, 9, 19–22])

$$F(q) = \int \frac{d^3\mathbf{k}}{4\pi/3} n(k) n(|\mathbf{k} + \mathbf{q}|). \quad (7)$$

The HF-function exhibits the following properties

$$\int \frac{d^3\mathbf{q}}{4\pi/3} F(q) = 1, \quad F(q \rightarrow \infty) \sim 1/q^8, \quad (8)$$

where  $F(0)$  is referred to as Löwdin number. Its lowest order expansion is

$$F_0(q) = \left[ 1 - \frac{3q}{4} + \frac{q^3}{16} \right] \theta(2 - q), \quad (9)$$

and its Fourier transform follows from the 1-matrix in  $r$ -representation

$$f(r) = \int_0^\infty d(k^3) \frac{\sin kr}{kr} n(k) \Rightarrow \int_0^\infty d(q^3) \frac{\sin qr}{qr} F(q) = [f(r)]^2. \quad (10)$$

This shows, that  $S_p$  splits quite naturally into a reducible HF-part  $S_p^{\text{HF}} = 1 - F$  [which needs the knowledge of the correlated  $n(k)$ ] and a non-reducible cumulant remainder  $S_p^{\text{cum}} = S_d - S_x$  as in Eq. (6) in agreement with the linked-diagram theorem [23]:  $S_{d,x}$  are sums of linked diagrams, the unlinked ones are in the HF term. In addition to the norms (1), (3) and (8), it holds

$$\int_0^\infty d(q^3) [S_d - S_x](q) = 0, \quad \int_0^\infty dq q^4 [S_d - S_x](q) = \frac{3}{4}t - g_p''(0)$$

The analogous splitting of the PCF is  $g_p = g_p^{\text{HF}} + g_p^{\text{cum}}$  with

$$g_p^{\text{HF}}(r) = 1 - [f(r)]^2, \quad g_p^{\text{cum}}(r) = \int_0^\infty d(q^3) \frac{\sin qr}{qr} [S_d - S_x](q). \quad (11)$$

The first equation only holds if the diagrams are completely summed up. The second equation states the Fourier transform relation between the cumulant part of the structure factor and that of the pair correlation function from which one can retrieve an approximation for  $g_p(r)$  given an approximation for  $S_d - S_x$ . Similarly, the splitting of the interaction energy is  $v_p = v_p^{\text{HF}} + v_p^{\text{cum}}$  with

$$v_p^{\text{HF}} = -\frac{\omega_{\text{pl}}^2}{4} \int_0^\infty d(k^3) \int_0^\infty d(k'^3) \frac{n(k)n(k')}{|\mathbf{k} - \mathbf{k}'|^2}, \quad v_p^{\text{cum}} = \frac{3\omega_{\text{pl}}^2}{4} \int_0^\infty dq [S_d - S_x](q) \quad (12)$$

with  $v_p^{\text{HF}} \rightarrow v_1 = -(3\omega_{\text{pl}}/4)^2$  for  $r_s \rightarrow 0$ , being HF in lowest order. [The index "1" means  $v_1 \sim r_s$ .] This analysis of Eqs. (1)-(12) is in agreement with the access through the 2-body reduced density matrix [4, 5]. By the way, this reconfirms vice versa the generalized Hellmann–Feynman theorem.

The asymptotics for  $q \rightarrow \infty$  is in first order (Kimbball trick [10])

$$S_d = -\left(\frac{g_a(0)}{q^4} + \frac{g_p''(0)}{q^6} + \dots\right) \omega_{\text{pl}}^2 + \dots, \quad S_x = -\left(\frac{g_a(0)}{q^4} + \frac{4g_p''(0)}{q^6} + \dots\right) \omega_{\text{pl}}^2 + \dots. \quad (13)$$

With Eq. (6) it is  $S_a = S_d$  and  $S_p = 1 + [S_d - S_x] + \dots$  or  $S_p = 1 + (3g_p''(0)/q^6) \omega_{\text{pl}}^2 + \dots$ , see [12]. So  $S_p(q \rightarrow \infty)$  starts with a  $1/q^6$ -term, while the total SF  $S = S_a + S_p$  starts with a  $1/q^4$ -term, approaching zero from below. The quantities  $1 - g_a(0) = 0.7317 r_s + \dots$  [11]

and  $2/5 - g_p''(0) = 0.2291 r_s + \dots$  [13] are correlation measures, vanishing for  $r_s \rightarrow 0$  and increasing with  $r_s$ . For  $r_s \rightarrow 0$  the correlation induced cumulant parts vanish and it remains (the uncorrelated) HF in lowest order:

$$S_p^{\text{HF}} \rightarrow S_0(q) = \left( \frac{3q}{4} - \frac{q^3}{16} \right) \theta(2-q) + \theta(q-2), \quad g_p^{\text{HF}} \rightarrow g_0(r) = 1 - \left( \frac{3(-r \cos r + \sin r)}{r^3} \right)^2. \quad (14)$$

The cusp singularities  $S_0(q \rightarrow 0) \sim q$  and  $\sim q^3$  make the non-oscillatory asymptotic terms of  $g_0(r \rightarrow \infty) \sim 1/r^4$  and  $\sim 1/r^6$  [24].

To gain information from the above Eqs. (1)–(14) the SFs  $F, S_{d,x}$  need to be known at least approximately. For  $S_{d,x}$  this is done within the RPA.

### A. Antiparallel-spin pairs: Coulomb hole in RPA

Fig. 1(c) shows the contribution to  $S_a$  in the lowest order of RPA:

$$S_{\text{ar}}(q) = -\frac{(3 \omega_{\text{pl}})^2}{4\pi} 2q \int_0^\infty du \frac{R^2(q, u)}{q^2 + q_c^2 R(q, u)}, \quad S_a = S_{\text{ar}} + \dots \quad (15)$$

The negative part of Fig. 5 shows  $S_a$  in RPA as a function of  $q$  and  $r_s$ . The index r denotes the RPA and the dots mean terms beyond RPA. Asymptotic properties: It has the small- $q$  asymptotics

$$S_a(q \rightarrow 0) = -\frac{1}{2} \cdot S_0(q) + \frac{1}{2} \cdot \frac{q^2}{2 \omega_{\text{pl}}} + \left[ d_4 \left( \frac{q}{\omega_{\text{pl}}} \right)^4 + d_5 \left( \frac{q}{\omega_{\text{pl}}} \right)^5 + \dots \right] \omega_{\text{pl}} + \dots \quad (16)$$

with the  $r_s$ -independent linear-cubic or ideal-gas term  $S_0$  of Eq. (14) and with a plasmon term  $\sim q^2$  (more precisely one half of it, the other half comes from  $S_p$ ). The  $r_s$ -dependent coefficients are in agreement with the bounds estimated by Iwamoto [25]. For  $r_s \approx 5$  it is  $d_4 \approx -0.0748$  and  $d_5 \approx +0.024$ .  $S_a(0) = 0$  corresponds to the perfect screening SR.  $S_a$  of Eq. (15) has the large- $q$  asymptotics  $\sim -(1/q^4 + 0.4/q^6 + \dots)$  as  $S_x$ . But cusp and curvature theorems demand a decoration by correlation parameters according to Eq. (13) beyond RPA.

Integral properties:  $S_a$  determines the antiparallel-spin PCF  $g_a$ , in particular the norm of  $S_a = S_d$  fixes the near-field correlation parameter  $g_a(0)$  in RPA [according to Eq. (1),

respectively Eq. (3) for  $r = 0$ ].  $S_{\text{ar}}$  of Eq. (15) in the interaction energy  $v_{\text{a}}$  of Eq. (2) gives

$$v_{\text{ar}} = -\frac{1}{2} \cdot \frac{27 \omega_{\text{pl}}^4}{8\pi} \int_0^\infty du \int_0^\infty d(q^2) \frac{R^2(q, u)}{q^2 + q_c^2 R(q, u)}. \quad (17)$$

For  $r_s \rightarrow 0$ , this behaves as  $v_{\text{a}} \rightarrow a \cdot x + \dots$  [with  $a = (1 - \ln 2)/\pi^2$  and  $x = (\alpha r_s)^2 \ln r_s$ ]. At  $q = 2$  the function  $S_{\text{ar}}(q)$  has an inflection point giving rise to the Friedel oscillations of antiparallel-spin electron pairs in the Fourier transformed pair correlation function.

### B. Parallel-spin pairs: Fermi hole beyond RPA

The exchange term  $S_x$  is part of the Fermi hole  $S_p$ , as seen from Eq. (6). The formula corresponding to Fig. 2(c) yields after a tedious derivation with contour integrations:

$$S_{\text{xr}}(q) = -3 \int \frac{d^3 \mathbf{k}_1 d^3 \mathbf{k}_2}{(4\pi)^2} \int_{-\infty}^{+\infty} \frac{k}{2\pi} \frac{k^2 u^2 + \varepsilon_1 \varepsilon_2}{(k^2 u^2 + \varepsilon_1^2)(k^2 u^2 + \varepsilon_2^2)} \cdot \frac{q_c^2}{k^2 + q_c^2 R(k, u)}, \quad (18)$$

with  $k_{1,2} < 1 < |\mathbf{k}_{1,2} + \mathbf{q}|$ ,  $\mathbf{k} = \mathbf{k}_1 + \mathbf{k}_2 + \mathbf{q}$ ,  $\varepsilon_1 = t(\mathbf{k}_2 + \mathbf{q}) - t(\mathbf{k}_1)$ ,  $\varepsilon_2 = t(\mathbf{k}_1 + \mathbf{q}) - t(\mathbf{k}_2)$ , and  $t(\mathbf{k}) = \mathbf{k}^2/2$ . One way to check this complicated integral is, to remove the screening term  $R(q, u)$  in the denominator. This yields the well-known energy denominator for the exchange term in lowest order,

$$S_{x1}(q) = -\frac{\omega_{\text{pl}}^2}{(4\pi/3)^2} \int \frac{d^3 \mathbf{k}_1 d^3 \mathbf{k}_2}{\mathbf{q} \cdot (\mathbf{k}_1 + \mathbf{k}_2 + \mathbf{q})} \frac{1}{(\mathbf{k}_1 + \mathbf{k}_2 + \mathbf{q})^2} \quad (19)$$

with  $k_{1,2} < 1 < |\mathbf{k}_{1,2} + \mathbf{q}|$ , as it should. We also verify this integral numerically as detailed in the Results section.

The exchange integral (19) has been calculated by Gutlé and Cioslowski [5, 26]. From (19) follows

$$S_{x1}(q \rightarrow 0) = -\frac{3}{4\pi} (2 \ln 2 - 1) r_s q + \dots$$

Unfortunately the integral in Eq. (18) is not known so far as an explicit function of  $q$  and  $r_s$ . It can, however, be evaluated numerically by means of an MC integration as described in the Results section. Note that in the SOSEX energy diagrams of Fig. 2(b) there are two types of interaction lines that can be cut out in order to retrieve a structure factor diagram. One is the interaction indicated by the left dashed line, connecting the exchanged Fermion loop. This type only contributes to the spin-parallel structure factor and exists starting from

second order. The other type of interaction is one that is contained in the RPA screened interaction, if that has at least one particle-hole bubble inserted. Thus, this type is less important since it only occurs from third order onwards. This type contributes equally to the spin-parallel as well as spin-antiparallel structure factor. As in the anti-parallel case, the function  $S_{\text{xr}}(q)$  has an inflection point at  $q = 2$  causing prominent Friedel oscillations for parallel-spin electron pairs as discussed in the Results section.

According to [1, 16] the high-density limits in lowest order of RPA

$$e = t_0 + v_1 + a \cdot x + \dots \quad \text{and} \quad v = v_1 + 2a \cdot x + \dots \quad (20)$$

hold [with  $a = (1 - \ln 2)/\pi^2$  and the shorthand  $x = (\alpha r_s)^2 \ln r_s$ ]. On the other hand it is  $v = v_a + v_p$  with Eqs. (2) and (17) and  $v_a = a \cdot x + \dots$ . This lets one expect  $v_p \rightarrow v_1 + a \cdot x + \dots$  for  $r_s \rightarrow 0$ .

The violation of the Pauli principle shows the need to search for further diagrams, which revoke or mitigate the deficiency. It remains to study whether and how the plasmon sum rule follows from (15) and (18). If  $S_x \rightarrow 3q/8 + q^2/(8\omega_{\text{pl}})$  for  $q \rightarrow 0$  and  $1 - F(q) = \mathcal{O}(q^3)$  holds, the plasmon sum rule  $S \rightarrow q^2/(2\omega_{\text{pl}})$  follows.

### III. RESULTS

We now turn to the numerical evaluation of the second order screened exchange structure factor  $S_{\text{xr}}(q)$  according to Eq. (18) and quantities derived from it, such as the second order screened exchange contribution to the spin-parallel pair distribution function. For a given momentum  $q$  we draw about  $10^6$  samples of the momenta  $\mathbf{k}_1, \mathbf{k}_2$  and the reduced imaginary frequency  $u$  for an MC evaluation of the 7-dimensional integral. The momenta  $\mathbf{k}_1$  and  $\mathbf{k}_2$  are sampled uniformly satisfying the integrand condition  $|\mathbf{k}_{1,2}| < 1 < |\mathbf{k}_{1,2} + \mathbf{q}|$ . Having drawn  $\mathbf{k}_1$  and  $\mathbf{k}_2$ , the reduced imaginary frequency  $u$  is drawn using importance sampling, distributed with a probability density function  $\text{PDF}(u)$  proportional to the term  $(k^2 u^2 + \varepsilon_1 \varepsilon_2)/((k^2 u^2 + \varepsilon_1^2)(k^2 u^2 + \varepsilon_2^2))$  occurring in Eq. (18), where  $\varepsilon_{1,2}$  and  $k$  follow from  $q$  and the drawn  $\mathbf{k}_{1,2}$ . The antiderivative of this PDF with respect to  $u$  can be expressed in closed form, note however, that its inverse must still be found numerically.

We verify Eq. (18) and above numerical procedure by computing the expectation value of the respective exchange contribution to the potential energy. This contribution can be

found either by computing the screened static structure factor  $S_{\text{xr}}(q)$  according to Eq. (18) and evaluating the expectation value of the bare Coulomb interaction  $q_c^2/q^2$  or, alternatively, by computing the bare dynamic structure factor  $S_{\text{x1}}(q, u)$  and evaluating the expectation value of the screened Coulomb interaction  $q_c^2 / (q^2 + q_c^2 R(q, u))$ . The bare dynamic structure factor is given by

$$S_{\text{x1}}(u, q) = -3 \int \frac{d^3 \mathbf{k}_1 d^3 \mathbf{k}_2}{(4\pi)^2} \frac{q^2 u^2 + \varepsilon_1 \varepsilon_2}{(q^2 u^2 + \varepsilon_1^2)(q^2 u^2 + \varepsilon_2^2)} \cdot \frac{q_c^2}{(\mathbf{k}_1 + \mathbf{k}_2 + \mathbf{q})^2}, \quad (21)$$

with  $\varepsilon_{1,2} = t(\mathbf{k}_{1,2} + \mathbf{q}) - t(\mathbf{k}_{1,2})$ . Note that  $\varepsilon_{1,2}$  is now decoupled for  $\mathbf{k}_{1,2}$ , as opposed to the case of the screened static structure factor  $S_{\text{xr}}(q)$  from Eq. (18), thus allowing  $\mathbf{k}_1$  and  $\mathbf{k}_2$  to be drawn independently for a given  $u$  and  $q$  with a probability density function  $\text{PDF}(\mathbf{k}_1, \mathbf{k}_2)$  proportional to  $|1/((\varepsilon_1 + i qu)(\varepsilon_2 - i qu))|$ . This is in contrast to evaluating  $S_{\text{xr}}(q)$ , where one can only efficiently draw  $u$  with a one dimensional  $\text{PDF}(u)$  proportional to a similar term, where  $q$  is replaced with  $\mathbf{k}_1 + \mathbf{k}_2 + \mathbf{q}$ . Both potential energies agree within numerical and statistical accuracy for all densities considered.

Fig. 5 shows the second order screened exchange structure factor for spin-parallel electrons as a function of  $q$  for different values of  $r_s$ . All error bars give the 95% confidence interval estimated from the variance of the integrand. The statistical uncertainty of the variance is estimated using the fourth central statistical moment. For comparison, Fig. 4 plots the RPA screened direct structure factor for spin-parallel electrons, showing that second order screened exchange contributes roughly half in magnitude to the total spin-parallel structure factor, however, with opposite sign.

In order to assess to which degree second order screened exchange improves on violations of the Pauli principle we evaluate the spin-parallel PCF  $g_p(r)$  from a Fourier transform of the spin-parallel structure factor  $[1 - F + S_{\text{dr}} - S_{\text{xr}}](q)$ . We approximate the HF-function  $F(q)$  from Eq. (7) using the uncorrelated momentum distribution  $n_0(k) = \theta(1 - k)$ , such that the HF-contribution to the spin-parallel structure factor evaluates to the well-known HF-Fermi hole  $g_p^{\text{HF}}(r)$  given in Eq. (14). The correlated part is calculated from a numerical Fourier transform of  $[S_{\text{dr}} - S_{\text{xr}}](q)$  according to Eq. (11). We use a Gauss–Kronrod rule for the numerical  $q$  integration with 32 subdivisions on each of the intervals  $(0, 1/8)$ ,  $(1/8, 1/4)$ ,  $(1/4, 1/2)$ ,  $(1/2, 1)$ ,  $(1, 2)$ ,  $(2, 4)$ ,  $(4, 8)$ , and  $(8, \infty)$ , totaling 3840 momentum samples. The last three intervals are transformed according to the asymptotic behavior of the cumulant part of the structure factor and the Fourier transform kernel  $q^2[S_{\text{dr}} - S_{\text{xr}}](q) \text{sinc}(qr) \sim 1/q^3$ .

Fig. 6 plots the resulting spin-parallel pair correlation function  $g_p(r)$  for selected densities compared to the uncorrelated Fermi hole  $g_p^{\text{HF}}(r)$ , indicated by the dotted graph. The inset enlarges the fluctuations around 1, showing the correlation effect on the Friedel oscillations in the random phase approximation with the second order screened exchange correction. To what extend SOSEX improves on the violations of the Pauli principle is demonstrated in Fig. 7 which contrasts the spin-parallel PCF in RPA+SOSEX, shown in bold, to the PCF in RPA without the SOSEX correction. The unphysical negative on-top value of the RPA is reduced to about one half by the SOSEX corrections. The remaining error stems from RPA ring diagrams of third or higher orders which posses exchange diagrams that are not part of the SOSEX correction. Fig. 7 also reveals that second order screened exchange strengthens the Friedel oscillations and makes them more density dependent.

#### IV. SUMMARY

The random phase approximation is the sum of all ring diagrams to infinite order. It becomes exact in the limit of high densities or, equivalently, at long distances. However, at intermediate and short distances RPA exhibits violations of the Pauli exclusion principle since RPA entirely lacks exchange, *i.e.* no two diagrams can be transformed into each other by exchanging Fermion lines at a Coulomb interaction. Such exchange diagrams correct for violations of the Pauli principle according to Wick's theorem.

For the pair correlation function or structure factor (SF) one has to distinguish electron pairs with antiparallel (a) and and parallel (p) spins. The spin-antiparallel SF  $S_a$  is within RPA well-known. The spin-parallel SF  $S_p$  proves to be a sum of a reducible HF-like term  $S_p^{\text{HF}}$  and a non-reducible cumulant remainder  $S_p^{\text{cum}}$ . This  $S_p^{\text{cum}}$  contains (besides  $S_a = S_d$ ) an exchange term  $S_x$ , whose second order screened exchange (SOSEX) approximation  $S_{xr}$  is calculated here for the first time numerically. Second order screened exchange considerably ameliorates the on-top spin-parallel PCF  $g_p(0)$ , roughly to half the negative value in the RPA without exchange correction. Compared to RPA only, the Friedel oscillations are also more prominent and more density dependent in RPA+SOSEX.

Beyond this work, it is also possible to compute  $n(k)$  in RPA+SOSEX. From that the kinetic energy  $t$  and the HF part of the structure factor and the PCF can be improved. Whereas the singular behavior of  $n(k)$  for  $k \rightarrow 1^\pm$  is known (in RPA), the special behavior

of  $S_{d,x}(q)$  for  $q \rightarrow 2^\pm$  [curvature jump, responsible for the  $r_s$ -dependent Friedel oscillations of  $g_{a,p}(r)$ ] is not known so far. Quite another question is, how the analysis presented here applies to recent attempts to split the Coulomb electron-electron repulsion into a short-range and a long-range part, see [27] and to use different approximations for these long- and short-range contributions to the exchange and correlation energy.

## ACKNOWLEDGMENT

The authors acknowledge P. Fulde and the Max Planck Institute for the Physics of Complex Systems Dresden for supporting this work and we thank the  $\Psi_{\mathbf{k}}$  community for helping to build fruitful cooperation as well as the DPG for their exciting Spring Meetings Dresden 2014 and Berlin 2015. Thanks also to J. Cioslowski, P. Gori-Giorgi, J.P. Perdew, and A. Savin for stimulating discussions.

## APPENDIX: MANY-BODY PERTURBATION THEORY PAR FORCE

MBPT theory shows that the ground state energy  $e$  is given by all linked Feynman diagrams. The building elements of linked diagrams are directed Fermion lines  $G_0(k, \omega)$ , which contain  $t(\mathbf{k}) = k^2/2$ , connected by dashed Boson interaction lines  $v(\mathbf{q}) = q_c^2/q^2$ . The number of interaction lines gives the order of the energy-diagram under consideration. In a homogeneous system each line carries one momentum and momentum is conserved at each vertex, which is where an interaction line meets an incoming and an outgoing Fermion line. The quantum kinematics, encoded in the momentum distribution  $n(k)$ , and the structure factor  $S(q)$  can be found from  $e$  by the (generalized) Hellmann–Feynman theorems according to Eq. (4) and Eq. (5), respectively. For  $n(\mathbf{k})$ , Eq. (4) yields the well-known Migdal formula  $n(\mathbf{k}) = \int d\omega/2\pi i \ G(\mathbf{k}, \omega)$ . The quantities  $n(k)$  and  $S(q)$  can be considered as 2 different “projections” of the linked diagram under consideration. In Eq. (4) one particle-hole line is cut out and in Eq. (5) an interaction line is cut out. Both procedures produce open diagrams. For the functional derivatives see App. A [18]. A theorem related to Eq. (5) is the virial theorem  $v = r_s de/r_s$  [16]. Note that the approximations for  $e, t, v$  must use the

same diagrams to be consistent in the sense that  $e = t + v$ .

---

- [1] W. Macke, Z. Naturforsch. A **5**, 192 (1950). Another approach with the same result is due to D. Bohm and D. Pines (1953).
- [2] P. Ziesche, J. Tao, M. Seidl, and J.P. Perdew, Int. J. Quantum Chem. **77**, 819 (2000).
- [3] For the history of the cumulant concept in Statistical Physics and Many-Body theory see *e.g.* P. Ziesche and refs. therein in J. Cioslowski (Ed.), Many-Electron Densities and Density Matrices, p. 34, Kluwer/Plenum, New York (2000). A survey on RDMs in quantum chemistry and their cumulant representation is in W. Kutzeligg and D. Mukherjee, Int. J. Quantum Chem. **110**, 2800 (1999) and in K. Kladko and P. Fulde, Int. J. Quantum Chem. **66**, 377 (1998). A novel interpretation of RDMs and their cumulants is in L. Kong and E.F. Valeev, J. Chem. Phys. **134**, 214109 (2011); for attempts to use quantum-chemical methods also for solid-state calculations see P. Fulde, Nature Physics **12**, 106 (2016); see also G. H. Booth *et al.*, Nature **493**, 365 (2013).
- [4] P. Ziesche, Phys. Rev. A **86**, 012508 (2012); A **89**, 059902(E)(2014).
- [5] P. Ziesche and J. Cioslowski, J. Modern Phys. **5**, 725 (2014). - The paragraph with Eq. (4.11) proves to be omitted.
- [6] M. Gell-Mann and K. Brueckner, Phys. Rev. **106**, 364 (1957).
- [7] L. Onsager, L. Mittag, and M.J. Stephen, Ann. Physik (Leipzig) **18**, 71 (1966).
- [8] E. Daniel and S.H. Vosko, Phys. Rev. **120**, 2041 (1961).
- [9] I.O. Kulik, Z. Eksp. Teor. Fiz. **40**, 1343 (1961) [Sov. Phys. JETP **13**, 946 (1961)].
- [10] J.C. Kimball, Phys. Rev. A **7**, 1648 (1973).
- [11] J.C. Kimball, Phys. Rev. B **14**, 2371 (1976).
- [12] A.K. Rajagopal, J.C. Kimball, M. Banerjee, Phys. Rev. B **18**, 2339 (1978).
- [13] V.A. Rassolow, J.A. Pople, and M.A. Ratner, Phys. Rev. B **59**, 2232 (2000).
- [14] D. Freeman, Phys. Rev. B **15**, 5512 (1977).
- [15] J. Goldstone, Proc. Roy. Soc. A 239.1217, pp. 267-279. (1957)
- [16] N.H. March, Phys. Rev. **110**, 604 (1958). For  $e(r_s)$  see *e.g.* H. Cong, phys. stat. sol. (b), **205**, 543 (1998).

- [17] P. Gori-Giorgi, F. Sacchetti, G.B. Bachelet, *Physica A* **280**, 199 (2000); *Phys. Rev. B* **61**, 7353 (2000); *Phys. Rev. B* **66**, 159901(E)(2002).
- [18] P. Ziesche, *Ann. Physik (Berlin)* **522**, 739 (2010).
- [19] P. Gori-Giorgi and P. Ziesche, *Phys. Rev. B* **66**, 235116 (2002).
- [20] V. Olevano *et al.*, *Phys. Rev. B* **86**, 195123 (2012).
- [21] M. Holzmann *et al.*, *Phys. Rev. Lett.* **107**, 110402 (2011).
- [22] S. Huotari *et al.*, *Phys. Rev. Lett.* **105**, 086403 (2010).
- [23] P. Ziesche, *Commun. Math. Phys.* **5**, 191 (1967).
- [24] P. Ziesche, *phys. stat. sol. (b)* **242**, 2051 (2005).
- [25] N. Iwamoto, *Phys. Rev. A* **33**, 1940 (1986), Eq. (4.2)
- [26] C. Gutlé, *Comp. Phys. Commun.* **174**, 836 (2006). The marked simplification for  $q \geq 2$  is due to J. Cioslowski [5].
- [27] P. Gori-Giorgi and A. Savin, *Phys. Rev. A* **73**, 032506 (2006), A. Savin, *Chem. Phys.* **356**, 91 (2009).
- [28] T. Chachiyo, *J. Chem. Phys.* **145**, 021101 (2016) and V.V. Karasiev, *J. Chem. Phys.* **145**, 157101 (2016).
- [29] P.K. Aravind, A. Holas, and K.S. Singwi, *Phys. Rev. B* **25**, 561 (1982).
- [30] F. Brosens, J.T. Devreese, and L.F. Lemmens, *Phys. Rev. B* **21**, 1363 (1980); J.E. Alvarellos and F. Flores, *J. Phys. F: Met. Phys.* **15**, 1929 (1985); B. Holm and U. von Barth, *Phys. Rev. B* **57**, 2108 (1998).
- [31] P. Fulde, *Nature Physics* **12**, 106 (2016);
- [32] G. Booth *et al.* *Nature* **493**, 365 (2013).

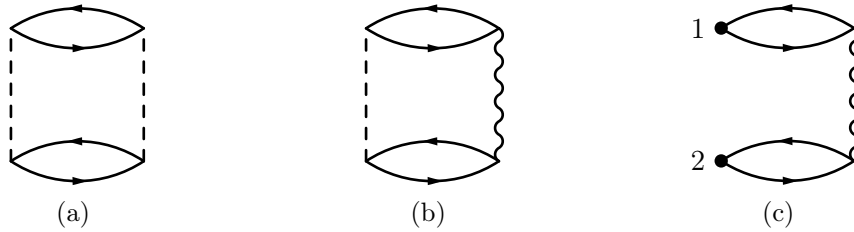


FIG. 1. (a) Linked energy diagram of second order. This diagram diverges for the homogeneous electron gas. (b) Finite linked energy diagrams of the random phase approximation (RPA). Note that the wiggly screened interaction line contains zero to infinite insertions of a particle-hole bubble connected by one to infinite bare (dashed) interaction lines. (c) Cutting one interaction line yields the diagrams of the RPA screened structure factor  $S_{\text{dr}}$ . Also note that all interactions lines are equivalent and which one is represented by the dashed line is arbitrary.

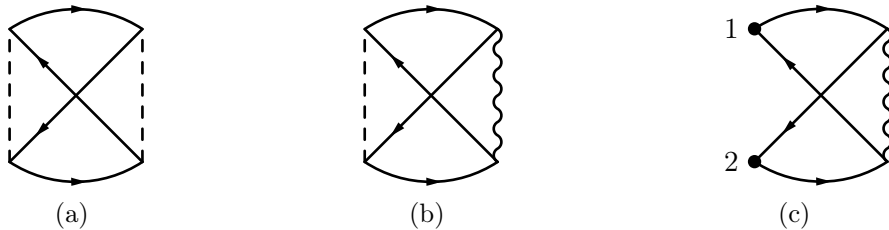


FIG. 2. (a) Linked energy diagram of second order from exchanging two Fermion lines of Fig. 1(a). (b) Linked energy diagrams of the second order screened exchange correction (SOSEX) by screening one of the two interactions of (a). (c) Cutting out the dashed interaction line yields the dominant diagrams of the SOSEX structure factor for parallel electrons  $S_{\text{xr}}$ . Note that one can also cut one of the interactions contained in the wiggly RPA screened interaction.



FIG. 3. In this term there are no links between the left and the right half. They can be summed up to give the HF-function  $F(q)$ .

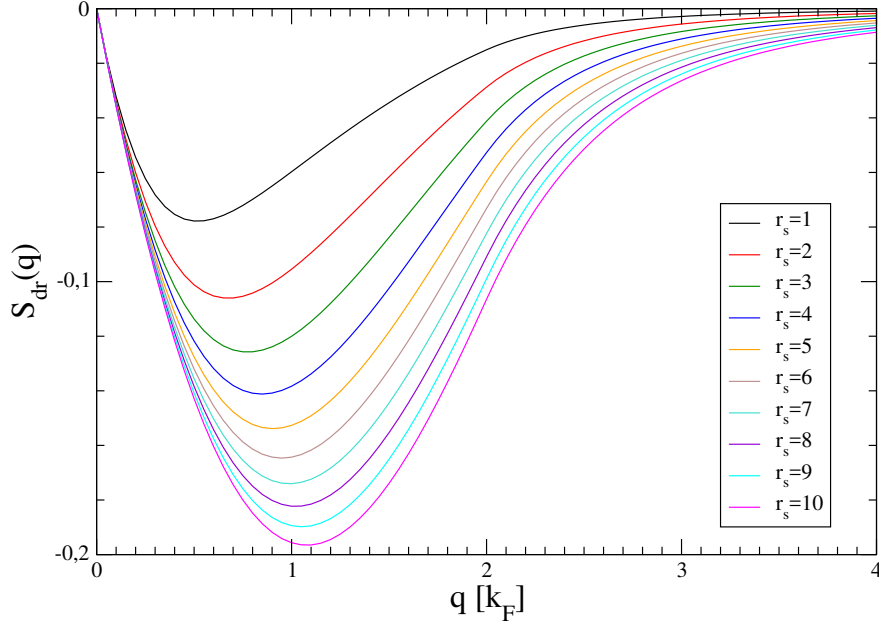


FIG. 4. Direct structure factor in RPA according to Eq. (15), evaluating the diagram in Fig. 1(c). Note the inflection points at  $q = 2$ .

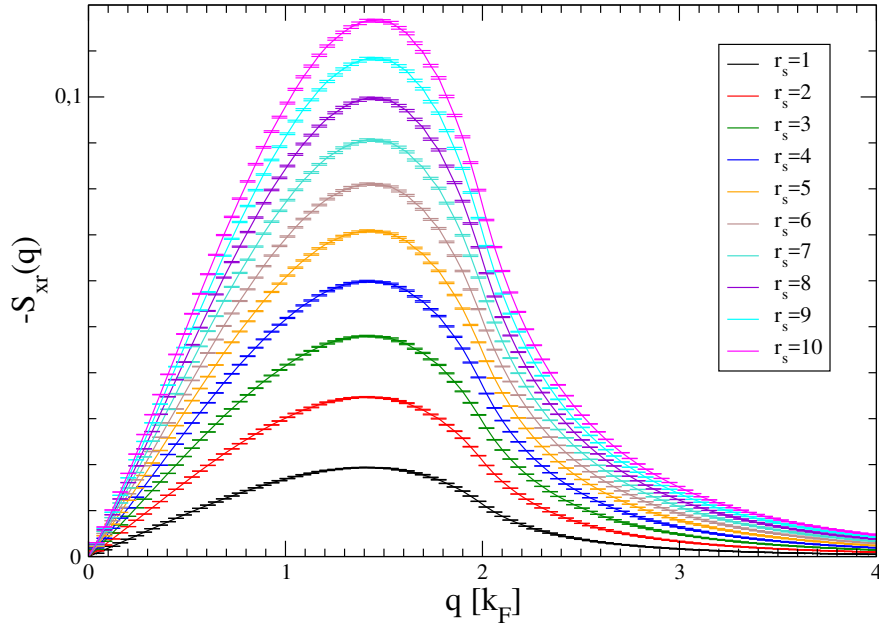


FIG. 5. Second order screened exchange structure factor in RPA according to Eq. (18), evaluating the diagram in Fig. 2(c). It contributes roughly half as strongly to the total structure factor compared to the direct contribution, however, it has opposite sign. Note the inflection points at  $q = 2$ . The error bars show the 95% confidence interval of the MC integration.

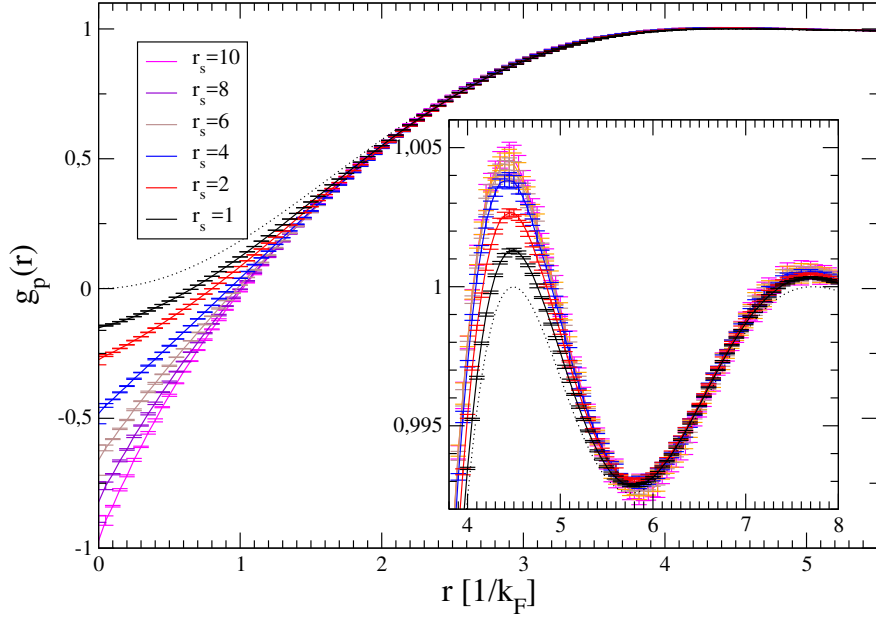


FIG. 6. Pair correlation function (PCF)  $g_p(r)$  for electrons of parallel spins in the random phase approximation (RPA) including the second order screened exchange (SOSEX) correction. The dotted HF part is computed from the uncorrelated momentum distribution  $n_0(k) = \theta(1 - k)$ .

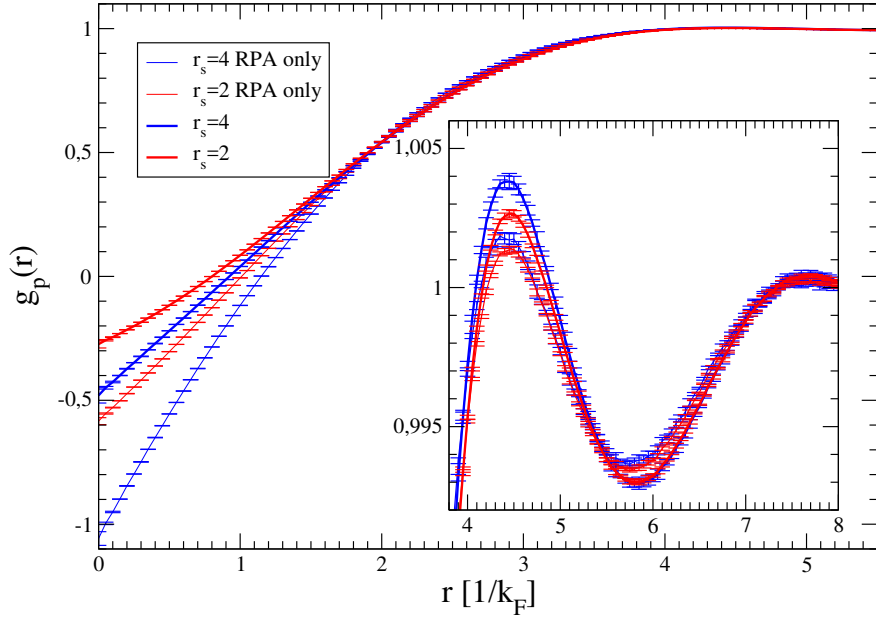


FIG. 7. Comparison of the PCF  $g_p(r)$  for electrons of parallel spins in the RPA with (thick) and without (thin) SOSEX correction. Exchange considerably improves on the unphysical negative part close to the coalescence point  $r = 0$ . Its effect on the Friedel oscillations are shown in the inset.